On the hindlimb biomechanics of the avian take-off leap

E. A. Meilak[1,2], P. Provini[3], C. Palmer[2], N. J. Gostling[4,6], M. O. Heller[1,5,6]

1. Bioengineering Research Group, Faculty of Engineering and Physical Sciences, University of Southampton, Southampton, UK; 2. Faculty of Environmental and Life Sciences, University of Southampton, Southampton, UK; 3. Université de Paris, INSERM U1284, Center for Research and Interdisciplinarity (CRI), F-75006 Paris, France; 4. School of Biological Sciences, Faculty of Environmental and Life Sciences, University of Southampton, Southampton, UK; 5. Centre for Sport, Exercise and Osteoarthritis Research Versus Arthritis, Southampton, UK; 6. Institute for Lifesciences, University of Southampton, Southampton, UK

Correspondence:

Corresponding author

Prof. Dr.Markus O. Heller

University of Southampton

Faculty of Engineering and Physical Sciences

Department of Mechanical Engineering

Southampton

SO17 1BJ

United Kingdom

m.o.heller@soton.ac.uk

Abstract

Although extant land birds take to the air by leaping, generating the initial take-off velocity primarily from the hindlimbs, the detailed musculoskeletal mechanics remain largely unknown. We therefore simulated *in silico* the take-off leap of the zebra finch, *Taeniopygia guttata,* a model species of passerine, a class of bird which includes over half of all extant bird species. A 3D computational musculoskeletal model of the zebra finch hindlimb, comprising of 43 musculotendon units was developed and driven with previously published take-off ground reaction forces and kinematics. Using inverse dynamics, the external moments at the ankle, knee, and hip joints were calculated and contrasted to the cumulative muscle capability to balance these moments. Mean peak external flexion moments at the hip and ankle were 0.55 bodyweight times leg length (BWL) each whilst peak knee extension moments were about half that value (0.29 BWL). Muscles had the capacity to generate 146%, 230%, and 212 % of the mean peak external moments at the hip, knee, and ankle, respectively. Similarities in hindlimb morphology and external loading across passerine species suggest that the effective take-off strategy employed by the zebra finch may be shared across the passerine clade and therefore half of all birds.

Introduction

Take-off is a crucial part of avian flight, requiring energy-intensive motion to accelerate into the air. Understanding how birds make the transition from standing statically to being airborne is one of the key components necessary for understanding how avian flight evolved. Previous work on the take–off of a variety of land birds demonstrated that the hindlimb plays a major role in propelling the bird in to the air, and suggests that the bipedal leap generates approximately 80-90% of the take-off velocity [1-6]. The group Passeriformes (passerines) includes over 5000 species of bird, making up approximately 60% of all bird species [7-9]. Among them, the zebra finch (*Taeniopygia guttata*), a frequently utilised model species, is also known to primarily use its hindlimbs to take to the air: previous studies showed that the hindlimb is responsible for producing 94% of their take-off velocity [2]. To date however, the detailed internal hindlimb mechanics necessary to produce a successful take-off remain largely unknown. This lack of knowledge in extant birds not only limits our understanding about how they master the feat of taking to the air but also presents an obstacle to accurately infer the capacity of fossil birds to be airborne, thus blurring our understanding of the origin of flight more generally.

Computational biomechanical modelling is a useful tool for calculating the internal mechanics occurring within a biomechanical system which are otherwise very difficult if not impossible to directly measure [10-15]. Moreover, the application of such computational analysis methods to extant animals is seen as a key strategy to systematically develop the sound biomechanical basis on which to further our understanding also of the conditions in extinct species [16-18]. The inverse analysis approach is one such computational method that takes measured kinematics and kinetics to drive a biomechanical model to calculate the internal moments at each degree of freedom of each joint [14, 19-22]. Detailed, 3D models of the musculoskeletal anatomy allow relating these external moments to the moment generating capacity of the internal force generating structures, i.e. the muscles, and to develop a more detailed understanding of internal avian hindlimb kinetics during the take-off leap. However, few

studies have reported on the detailed external kinetics (ground reaction forces) [2, 4-6] associated with the avian take-off leap and even fewer studies have investigated 3D hindlimb kinematics for these activities [1]. The authors are aware of only a single study that has investigated the biomechanics of the avian jump, focussing on a predictive simulation of the ground dwelling elegant-crested tinamou *Eudromia elegans* [23]. However, due to the scarcity in ground reaction forces and kinematic data of the tinamou leap, data on which an inverse analysis would rely on, the authors opted for a forward approach to predict the leaping behaviour. In how far the simulations reflect kinetics and kinematics that are consistent with actual conditions that can be observed and measured in this bird therefore remains to be established. Although computational analyses in birds are available and have shown the value of such analyses to further our understanding of avian hindlimb biomechanics with respect to e.g. the critical role of the ankle muscles in the take-off leap of the tinamou and the function of the antitrochanter as a passive mechanism to stabilise the hip of the running ostrich [23, 24], to date no study has determined the internal hindlimb joint kinetics of a flying bird as it leaps into the air using detailed measurements of external forces and hind limb kinematics. With the application of X-ray reconstruction of moving morphology (XROMM) technology to capture detailed 3D bone kinematics of the avian take-off leap, in combination with computational biomechanical analyses, the technology is finally available to accurately simulate the internal mechanics of the extant avian take-off [1, 10, 16, 25-28].

The current study therefore combines external forces and detailed bone kinematics that feed into computer simulations into the biomechanics of the hindlimb throughout the take-off leap of the zebra finch. In doing so we aim to address the following hypotheses that help to develop a comprehensive understanding of the mechanical requirements birds need to meet to propel themselves into the air. We firstly hypothesised that in order to generate the motion of the avian take-off leap, characterised by the hip, knee, and ankle joints all extending until the bird is airborne [1, 3], net external flexion moments of similar peak magnitudes act at all these joints which the muscles balance by exerting extension moments. Consistent with the observation that predicative simulations of the tinamou

88 predict the ankle to be most critical in determining the success of the take-off leap in a ground-
89 dwelling bird [23], we further hypothesised that the ankle extensors of the zebra finch possess the
90 largest capacity to balance the external moments. Finally, considering the avian hips' powerful
91 capacity to generate internal/external rotation (IER) moments and a poor capacity to generate
92 abduction/adduction (ABAD) moments [10, 16, 24] in the presence of the antitrochanter, we
93 hypothesise that external moments of similar peak magnitudes act in IER/ABAD on the hip joint of the
94 zebra finch and that the bird possess powerful ability to actively balance the IER moments.

95

Materials and methods

To address our hypotheses, we built upon previously published detailed kinetics and kinematics data of the take-off leap of the zebra finch as input to a biomechanical simulation of the avian take-off leap [1, 2] as explained in more detail below.

Overview

Key steps of our analysis methodology included the use of CT scans of the same individual, together with additional morphological data in the literature to characterise the bone and musculature respectively, from which a detailed 3D musculoskeletal model of the zebra finch hindlimb was developed. Here, muscles were mapped from a previously published magpie musculoskeletal model on to the zebra finch skeleton [10, 29, 30]. In addition, previously published 3D kinematics and ground reaction forces were used to drive the musculoskeletal model in inverse dynamics analyses to estimate external joint moments [1, 2]. The combination of these unique datasets, collected from the same species and even the same individual, offered a unique opportunity to generate an accurate simulation of the zebra finch take-off biomechanics.

The external joint moments were compared against the moment generating capacity of the muscles to document the biomechanical requirements and to assess the zebra finch's capability to actively balance the hindlimb joint moments experienced throughout the take-off leap. Here, moments about hip flex/extension (FE), ab/adduction (ABAD), int/external rotation (IER) and moments about FE at both the knee and ankle joints were considered. In addition, by comparing the hindlimb morphology and ground reaction forces of a variety of passerines ranging in mass (zebra finch *Taeniopygia guttata*, 15.4 g, starling *Sturnis vulgaris*, (77.3 g), crow *Corvus corone* (440 g) and raven *Corvus corax*, 1.1 kg) it was possible to explore the take-off mechanics of passerines more generally.

Materials, model building, and musculoskeletal analysis approach

The computational biomechanical musculoskeletal model of a zebra finch (15.4 g) was developed based on CT scans and muscle data of corvids from previously published works [1, 10, 29]. The CT data

was used for establishing the 3D skeletal model. In order to describe the spatial relationships between bones, local coordinate systems were established based on shape fitting techniques and functional analyses of the joints [31], as detailed in the supplementary information (S1A). Muscles were modelled by 3D lines of action [12, 32, 33] by mapping muscles from the magpie skeleton to the zebra finch using elastic registration [34], while muscle maximum isometric force was scaled by body mass. Detailed kinematics derived from previously published XROMM data [1] were then used together with ground reaction forces [2] of zebra finch take-off leaps to drive the model in inverse dynamics simulations to calculate the external moments acting at the hindlimb joints. Nine sets of ground reaction forces obtained from 9 jumps of 4 birds (15.4±1.8g), were temporally synchronised with two sets of kinematics trials (taken from 1 bird with a mass of 15.4 g), resulting in 18 simulations analysed. Muscle moment arms were measured and used to calculate the maximum moment generating capacity about hip flexion/extension, ab/adduction and internal/external rotation, and knee and ankle flexion/extension. The muscle moment generating capacity was compared to the external joint moment to ascertain the zebra finch's ability to balance the external joint moments.

Skeletal model

The skeletal model was derived from CT scans (isotropic resolution 0.04mm) of a zebra finch *Taeniopygia guttata* specimen (15.4 g), obtained in previously published studies (for full details please refer to [1]). For the current study, bones were segmented using ITK-SNAP [35], and imported in to Rhino (v7; Robert McNeel & Associates, Seattle, USA) [36] where triangulated bone surfaces were obtained after fitting subdivision surfaces using the QuadRemesh function. Bones which were treated in this way were the pelvis, femur, patella, tibiotarsus and tarsometatarsus. The detailed definition of joint centres and axes and local bone coordinate systems are available in the supplementary information (S3).

A linked rigid body model with 4 segments including the pelvis, thigh, shank and tarsometatarsus was defined in OpenSim v4.1 [37]. Here, body segments were linked by 3 joints (hip, knee and ankle joints)

with 3 rotational degrees of freedom (DoF) at the hip (allowing flexion/extension, internal/external rotation and ab/adduction) and 2 DoF at each of the knee and ankle joints (allowing flexion/extension and internal/external rotation). Because the foot remained stationary on the perch and motion of the trunk was largely due to the extension of the hip, knee and ankle joints, the foot was not included as a dedicated structure of the musculoskeletal model. In order to better capture the mechanics of hindlimb extension, a biomechanical model of the patella-femoral joint was incorporated in to the model. Here, the motion of the patella was defined by a 3D spline curve following approximately the trochlear surface of the femur. The patella was allowed to move along that spline as a function of the knee angle, with details of the motion informed by a musculoskeletal model of the helmeted guineafowl *Numida meleagris* [38]. In order to map patellar motion from the guineafowl to the zebra finch model, the femoral surface of the guineafowl model was elastically registered to the zebra finch femur [39]. The parameters of the elastic registration were then used to map the spline defining patellofemoral motion from the guineafowl to the zebra finch model using the R-package MesheR [34].

Muscle geometry

The musculoskeletal model of the zebra finch included 43 muscles crossing the hip, knee and ankle, which were modelled as 3D polylines spanning origin and insertion using via points to fully describe their curved paths (Figure 1). Magpies (*Pica pica*) and zebra finch, share broadly similar hindlimb myology both following the characteristic hindlimb morphology of passerine birds [9]. Muscle attachment sites and via points were therefore mapped from a previously established model of the magpie [10] to the zebra finch hindlimb. Using a non-rigid iterative closest point (ICP) registration [39] the magpie femur, tibiotarsus and tarsometatarsus were elastically registered to the corresponding long bones of the zebra finch hindlimb [34] (Figure 2). Using 3D Slicer 4.11 [40], the pelvis of the magpie and zebra finch were first split in to the ilium, ischium and pubis before elastically registering them onto each other following the same approach as described for the long bones above. Following non-rigid registration, the rigid transformation and isotropic scaling parameters were recovered using

Ordinary Procrustes Analysis (OPA) [41] computed between the vertices of the original magpie bone surface and the vertices of the magpie bone surface that was elastically registered to the respective zebra finch bone (Matlab (2019b, The Mathworks, Nantucket, USA). This step was encoded in a 4x4 homogeneous transformation matrix. The remaining difference between the positions of the OPA mapped vertices and their elastically registered counterparts was captured in a dense deformation field. The homogeneous transformation matrix and the dense deformation field were then applied to all attachment and via points of the magpie muscles associated to the respective bone surface using the R-package MesheR [34], and in so doing mapping muscles from the magpie hindlimb to the zebra finch (Figure 2). Wrapping cylinders and spheres were added with positions, orientations and radii individually adjusted to define the 3D muscle paths throughout the jumping RoM that avoided any intersection of muscles with bones.

Biomechanical analysis

Kinematics

Detailed 3D kinematics were derived from previously published X-ray reconstruction of moving morphology (XROMM) data of the left hindlimb throughout two autonomous take-off leaps of the zebra finch [1]. For these analyses three tantalum bead markers with an approximate diameter of 0.5 mm were attached to the tarsometatarsus, while two markers were implanted to the tibia, one to the femur, and one at the pelvis. In order to reliably track 3D skeletal kinematics for the current study, the location of the pelvis was determined using the implanted pelvic marker and, while its orientation was determined using scientific rotoscoping, a reliable process in particular for bones with specific shapes such as the pelvis [42]. Owing to the generally higher precision of the 3D marker positions compared to 3D position and orientation data derived from scientific rotoscoping [1, 42], a method for reconstructing 3D skeletal motion that maximised usage of the marker data while minimising reliance on the manual process of scientific rotoscoping was developed. Here, 3D positions and orientations of the long bones of the hindlimb were obtained using the attached physical markers, supplemented

by functionally defined virtual markers, and detailed 3D bone surface models. A full detailed description of the methodology used to define these virtual markers and track 3D skeletal motion using a combination of XROMM data, bone surfaces and virtual markers is provided in the supplementary materials section (S1, S2).

An inverse kinematics analysis was then carried out in OpenSim [22, 32, 37] to map the kinematics from the XROMM data to the constrained biomechanical model using physical and virtual markers placed at their known locations on the model bones. Across the two kinematics trials, the ranges of motion for the skeletal kinematics with respect to hip flexion/extension (FE), abduction/adduction (ABAD) and internal/external rotation (IER) recovered in that manner were 42° (-4° to 38°), 15° (-37° to -22°), and 20° (8° to 28°), respectively. Knee and ankle FE range of motion were 40° (123° to 163°) and 74° (61° to 135°), respectively (see supplementary figure SF1). Substantial internal/external rotation range of motion at the knee and ankle was also measured, with a range of motion of 16° (5° to 21°) and 30° (-15° to 15°), respectively.

The take-off velocity of the bird was defined by measuring the velocity of its centre of mass at the instant the feet left the ground [2, 3, 6]. To that end, the centre of mass of the zebra finch was determined using the soft tissue envelope of the zebra finch and the RigidBodyParams [43] function under the assumption of a homogenous body soft tissue density [43]. The velocity of the centre of mass of the zebra finch was then measured by tracking its location throughout the take-off trials using the OpenSim 4.1 BodyKinematics Tool. Take-off velocity was determined as the velocity at the instant all toes on the hindlimb being tracked, left the perch. Take-off velocities for the two trials investigated were determined to be 1.39 and 1.08 m/s.

Kinetics

Previously reported ground reaction forces of the take-off leap of a zebra finch [1] were used as inputs to the current study in this study. Since full details for the collection of these data were previously reported, the experimental setup is only briefly summarized below. Vertical and horizontal ground

222 reaction forces were recorded at 400 Hz from a force platform (Squirrel force plate, Kistler France, Les
223 Ulis, France; resolution ±0.01N), to which a wooden perch, 1.5 cm in diameter, was attached. The
224 ground reaction forces measured from nine trials of a zebra finch taking off from a perch [2] were
225 used to drive the take-off simulations.

226 Each of the nine zebra finch kinetics trials were paired with the two sets of kinematics trials enabling
227 analysis of 18 distinct take-off conditions. Here, the ground reaction forces were temporally aligned
228 to the kinematic data such that at the instant at which the resultant ground force fell to zero was
229 matched to the instant at which the toes left the ground. Ground reaction forces were assumed to act
230 through the centre of the perch (Figure 3).

231 For use in the current study, the ground reaction force vectors were scaled in magnitude so that the
232 impulse imparted by the leg resulted in 94% take-off velocity that was measured from the kinematics
233 for the two trials considered here. This scaling was performed to reflect previously identified
234 relationships for the take-off mechanics of the zebra finch [2]. Here, the method for calculating the
235 velocity as a result of the impulse (V_{GRF}) imparted by the hindlimb followed the approach by Provini
236 and colleagues (2012) and is outlined below. Firstly, the acceleration resulting from the ground
237 reaction forces, $\dot{V}_{GRF}$, were calculated as follows:

238 $$\dot{V}_{GRF} = \frac{\sqrt{F_x^2 + F_y^2 + (F_z^2 - mg)}}{m} \qquad (2)$$

239 where F_x is forward force, F_y is lateral force, F_z is vertical force, m is the mass of the bird, and g is the
240 acceleration due to gravity. The integral of the acceleration over the duration of the take-off then
241 provides the take-off velocity as a result of the ground reaction forces, V_{GRF}:

242 $$V_{GRF} = \int_{t_0}^{lo} \frac{\sqrt{F_x^2 + F_y^2 + (F_z^2 - mg)}}{m} dt \qquad (3)$$

243 where t_0 is the time when the jump starts and lo the time at lift off.

External joint moments

Ground reaction forces were applied to the tarsometatarsus, with the centre of pressure placed in the centre of the perch (Figure 3). Using kinematics and ground reaction forces as input to the inverse dynamics analysis, external joint moments were calculated about hip FE, ABAD, IER, knee FE and ankle FE. Joint moments were normalised by the product of bodyweight and leg length L (defined as the sum of the segment lengths of femur, tibiotarsus, tarsometatarsus, and digit III) [44], and time normalised to the duration of the jump cycle. Mean and standard deviations of the external joint moments were calculated across all 18 take-off sequences to obtain a robust estimate of the envelope of zebra finch take-off biomechanics. Here, joint moments are identified by the direction of joint movement induced by the action of the muscle group activating the respective degree of freedom.

Muscle moment generating capacity

The methodology for calculating muscle moment generating capacity followed the approach described by Meilak and colleagues (2021) and is outlined below. The moment generating capacity for each muscle about each joint degree of freedom (DoF) being considered was calculated by multiplying the muscle maximum isometric force (F_{max}) by the instantaneous moment arm ($MA_{t,i,j}$), evaluated at each time increment (t) throughout the kinematics trials. These moments were evaluated for each muscle *i (where i=1..43)* as the product of the maximum isometric muscle force (F_{max}) and the instantaneous moment arm ($MA_{t,i,j}$) determined throughout the take-off kinematics for each rotational DoF *j (where j=1..5* for hip FE, ABAD, IER, knee FE and ankle FE):

$$M_{t,i,j} = F_{max,i} \cdot MA_{t,i,j} \qquad (4)$$

The moments of muscles acting in the same direction (i.e. their moments have the same sign) were summed for each degree of freedom to provide the total joint moment generating capacity in relation to that specific action ($M_{t,j}$):

$$M_{t,j} = \sum_{i=1}^{43} M_{t,i,j} \qquad (5)$$

Comparing biomechanical conditions across the group of Passerine birds

To allow comparative analysis of conditions across the Passerine clade, the ground reaction force data available for the zebra finch was amended with similar data from further animals within the group of passerines. In a study approved by the local ethics committee of the University of Southampton (ERGO II ID 32207), a crow (*Corvus corone*) and raven (*Corvus corax*) took off 6 times each from a force platform (9260AA, Kistler) while 3D ground reaction forces (GRFs) were sampled at 10 kHz. For all species, vertical and horizontal forces were filtered using a zero-phase low-pass (40Hz) custom filter in Matlab. The peak ground reaction forces of the zebra finch, starling [3], crow and raven were all normalised by bodyweight and, together with key measures of hind limb geometry (Table 2) to compare take-off conditions within the group of passerines.

Results

The duration of the take-off leap ranged between 62-65ms (Figure 4). Mean resultant peak ground reaction forces per leg were 1.81±0.21 BW (range: 1.42 to 2.15 BW, c.f. supplementary figure SF1) and occurred at about 62 % leap cycle time. Across the two kinematics trials, the largest ranges of motions were 74°, 42° and 40° about the ankle, hip, and knee FE axes, respectively. The ranges of motion about the joints' secondary degrees of freedom were similar, with hip IER and ABAD RoMs of 20° and 15°, respectively and knee and ankle IER RoMs of 16° and 30°, respectively (see supplementary figure SF2).

The largest external moments observed were the moments around the flexion/extension axes. Here, the mean peak external joint flexion moments at the hip and ankle were of similar magnitude (0.66±0.04 and 0.68±0.05 BWL, respectively) while the mean knee extension moment was only about half that value (0.38±0.05 BWL, Figure 5, Table 3). The smallest peak moments were computed about hip IER and ABAD with mean peak moments of 0.27±0.07 and 0.20±0.07 BWL, respectively (Figure 5, Table 3). At the instances that these peak moments occurred, the muscles had the ability to generate 120%, 282% and 61% of the mean peak hip FE, IER and ABAD joint moments, respectively (Figure 5 Table 3). The muscles were able to generate 177% and 176% of the mean peak joint moments about the FE axes of the ankle and knee, respectively (Figure 5 B and C, Table 3).

Comparing conditions across the group of passerines, the zebra finch as bird with the smallest mass by far (15.4 g) had the smallest normalised peak ground reaction forces per leg of 1.94±0.25 BW, while starling (77.3 g), crow (440 g), and raven (1.1 kg) exerted very similar peak GRFs with values of 2.15±0.14 BW [3], 2.20±0.29 BW, and 2.25±0.14 BW, respectively (see supplementary figure SF3).

Discussion

This is the first detailed investigation into the hindlimb mechanics of a flying bird as it takes to the air with a take-off leap using modern biomechanical analyses. The model presented here simulated 18 distinct take-off trials of a zebra finch's take-off leap from a perch covering a range of take-off conditions in a passerine bird, the group that makes up approximately 60% of all extant bird species [7-9]. In doing so our study revealed a consistent pattern of internal mechanics across the trials that was characterised by the largest peak external moments occurring around the FE axis of the hip and ankle (requirements, 0.68 and 0.66 BWL, respectively), while considerably smaller external moments were observed about the FE axis of the knee, amounting to only 56% of the respective peak moments at the hip. On the other hand, peak hip IER and ABAD moments were 40% and 29% of peak hip FE moments respectively. Together with previous findings regarding the substantial extent of joint range of motion in IER exercised by birds [1, 27] and the substantial moment generating capacity of the hip joint muscles around that axis [10], these novel data on the internal hind limb mechanics during the take-off leap strongly support the notion that the execution and control of hindlimb motion in birds is not limited to a single (sagittal) plane but is essentially 3D in nature [16].

Across the hip, knee and ankle FE degrees of freedom, the muscles had the ability to generate 120%, 176%, and 177% of the mean peak external joint moments, respectively. In relative terms therefore, muscles spanning the hip were closest to reaching the capacity limit whilst muscles spanning the knee and ankle joints had the largest reserves. Although for the most typical (mean) of the conditions studied here the capacity of the muscles to generate moments was always larger than the requirement (Figure 5), the closing gap between the upper limit of the 2.5 SD range of the external hip flexion moments and available hip muscle extension capability suggests that more powerful take-off leaps than those observed here would likely require further activation of the more distal, knee and ankle joint spanning muscles for which the requirements remained more comfortably within their capability [23]. An explanation as to why capacity to balance the moments at the more distal joints

retains a larger reserve may be found in the design of the avian hindlimb and specifically the biarticular muscles [45-47]. Such biarticular muscles include in particular the m. caudofemoralis pars caudalis (MFCLP), m. flexor cruris medialis (MFCM) and m. iliofibularis (MIF) which span the caudal side of the hip and knee (Figure 1, Table 1). MFCLP and MFCM form a major part of the hip extensor moment generating capacity, together generating 35% of the total hip extensor moments whereas the MIF has a greater role as a hip abductor, generating 20% of the muscle abduction generating capacity [10]. Whilst during the take take-off leap of the zebra finch the hip, knee and ankle are all extending (Figure SF1), the muscles need to generate a net knee flexion moment, suggesting that knee flexors may be activated. Biarticular muscles, which if activated generate an extension moment at the hip but a flexion moment at the knee such as the MFCLP and MFCM, would thus appear to be prime candidates for meeting the demands during the take-off leap. Moreover, co-activation of knee flexors and extensor muscles (muscle co-contraction) though energetically less optimal, may help to increase compressive forces across the knee joint and help to lock or at least minimise the extent of internal/external rotation [27, 28, 48]. Further analysis to examine muscle activation patterns, though beyond the scope of the current work, could corroborate whether activation of these biarticular muscles to extend the hip and generate the extension moment applied to the knee suggested by the analyses here does indeed occur and help to further elucidate how avian hindlimb muscles are orchestrated during the take-off leap.

Here, it is also informative to consider absolute moments where indeed the ankle extensors had the largest joint moment generating capacity, capable of generating peak total extension moments of up to 1.18 BWL at the ankle, followed by the hip extensors, with a peak total capacity of 0.81 BWL. The passerine bird ankle muscles' capacity to produce the largest moments indicates the importance of the ankle joint throughout the take-off, a finding in line with previous research on the ground dwelling elegant-crested tinamou *Eudromia elegans* [23] where the take-off heavily depended on the parameters and activation of the ankle extensors. Though to the authors knowledge no similar studies reporting internal mechanics during a take-off leap of a flying bird are available for comparison, similar

350 analyses have been performed in ground-dwelling birds such as the emu and the ostrich. Here, data
351 on the running of the ostrich obtained using similar analysis methods revealed that the peak
352 normalised FE moments across all of the hip, knee, and ankle joint of the ostrich were considerably
353 smaller than those reported during the take-off leap of the zebra finch reported here. The largest
354 differences in normalised moment magnitudes were observed for the ankle and hip joints where the
355 peak moments during running in the ostrich amounted to only 24% (0.16 BWL) and 25% (0.17 BWL)
356 of the values for the zebra finch leap. The external moment at the knee during running in the ostrich
357 was the largest of all 3 hindlimb joints with 0.20 BWL yet amounted to only about 53% of the value
358 the current study calculated for the take-off leap of the zebra finch. In the comparison of the absolute
359 moment magnitudes it is important to consider that speed at which the ostriches were running was
360 rather slow (3.24 m/s) compared to the maximum speed ostriches can achieve (about 13.9 m/s) and
361 higher speeds will be associated with higher external forces and moments. However, not only absolute
362 magnitudes but also the ratios of their magnitudes at the hip, knee, and ankle differed between the
363 zebra finch take-off leap and ostrich running. While the largest external moment during running of the
364 ostrich was computed at the knee, suggesting that that ostrich running is knee driven, the external
365 knee moment during the take-off leap of the zebra finch was the smallest of all the hind limb joints.
366 For the zebra finch leap, peak moments were observed at the hip and ankle suggesting that this
367 motion is hip and ankle driven instead and signifying that an interesting avenue for future work would
368 be to investigate whether the different motor behaviours are indeed associated with different muscle
369 coordination patterns and that care must be taken when speculating about design principles and
370 interpreting optimality of the musculoskeletal system based on a limited repertoire of motor
371 behaviours.

372 Previous studies have demonstrated that avian pelvic muscles have a considerable capacity to produce
373 IER moments at the hip [10, 16, 49]. The current study revealed not only that substantial external
374 moments about the IER axis occur during the take-off leap of the zebra finch, approaching 40% of the
375 hip extension moment, but also demonstrated that the hip muscles had the greatest relative capacity

376 to actively balance these moments, with muscles capable of generating up to 280% of the mean peak
377 external IER moments. Together these data provide further evidence that IER rotation is actively
378 controlled during routine, straight line take-off leap of passerine birds. The ample capacity of the
379 muscles to enable IER during such jumps further allows for take-off leaps to occur with substantially
380 more axial turning/rotation while the bird remains on the ground, offering the bird a wider repertoire
381 of take-off and escape behaviours. On the other hand, foraging behaviours have been shown to be
382 linked with substantial extents of hindlimb IER [27] and it may well be that substantial IER capability
383 of the hip muscles are particularly crucial in supporting those behaviours (particularly for single limb
384 support) in addition to allowing variation in the take-off leap.

385 In contrast to the well powered hip IER DoF during the take-off leap, the pelvic muscles of the zebra
386 finch were only able to balance 61% of the peak mean external adduction moments. Analysis of the
387 relationship of the relative moment generating capacity of the avian hip muscles do indeed
388 demonstrate that the smallest capacity to generate a moment exists with respect to the ABAD axis.
389 However, even though the avian hip has a relatively limited capacity to actively produce hip ABAD
390 moments, birds can rely on a passive mechanism using the antitrochanter and associated ligamentous
391 structures to balance external abduction moments [49]. The utilisation of the antitrochanter is also a
392 feature in the hip mechanics of the ostrich: though substantial external abduction moments are
393 generated during walking and running in these flightless birds, the design of the hip allows to stabilise
394 the joint passively such that ostriches neither require nor possess muscles to do so actively [49, 50].
395 The antitrochanter is indeed a feature shared across all extant birds that was not present in some of
396 the very earliest birds such as *Archaeopteryx*, who likely relied on powerful hip adductors to generate
397 the required adduction moments [16].

398 Maintaining substantial lever arms of the muscles throughout the functional range of motion of a joint
399 is a prerequisite to maintain high levels of muscle capacity to generate moments. Passive structures
400 can play a key role to help maintaining muscle lever arms include sesamoid bones such as the patella

401 which is key to enable joint function in flexion at the knees in human and avian bipeds [33, 46] The
402 hypotarsus is another anatomical feature of the avian hindlimb that helps to guide tendons around
403 the ankle joint and to and maintain their lever arms [51]. The posterior side of the ankle further
404 includes the cartilagio tibialis which constrains the muscle line of action to act further away from the
405 joint axis of rotation thus helping to maintain its moment [29]. The model presented here therefore
406 modelled the patellofemoral joint in an approach informed by the birds' bone surface anatomy and
407 kinematic model data from the literature [38] and in incorporated these passive structures of the ankle
408 with wrapping objects and via points informed by CT scans.

409 The relative peak ground reaction forces during the take-off leap of all passerines considered here
410 were rather similar in magnitude, despite the large range in body mass. During the take-off leap the
411 zebra finch (15.4 g), starling (77.3 g), crow (440 g) and raven (1.1 kg) generated peak ground reaction
412 forces per leg of 1.94±0.25 BW, 2.15±0.14 BW [3], 2.2±0.29 BW, and 2.25±0.14 BW, respectively.
413 Similarities do not stop with the ground reaction forces but are also apparent in the morphology of
414 their hindlimbs. The passerines considered here, the zebra finch, starling, crow, and raven, possess
415 very similar hindlimb indices, a measure of relative segment lengths of the hindlimb ((tarsometatarsus
416 length + tibiotarsus length) / femur length [52]) with values of 2.64, 2.84, 2.75, and 2.63, respectively
417 [53] (Table 2). The similarities in normalised leg segment lengths and ground reaction forces spanning
418 a range of passerines, which differ in mass by approximately two orders of magnitude, support the
419 hypothesis that passerines share a similar take-off behaviour, as reported here. Forward dynamics
420 simulations of the tinamou (0.55 kg) leaping predict similar but somewhat higher peak ground reaction
421 forces of 2.62 BW per leg during the jump [23]. On the other hand, predicted joint kinematics profiles
422 for the take-off leap of the tinamou demonstrated ranges of motion at the hip knee and ankle of 65°,
423 91° and 109° respectively, consistently greater than the range of motion measured in the zebra finch
424 (42°, 40° and 74° respectively), while the hindlimb index of the tinamou *Eudromia elegans* (belonging
425 to the group Tinamiformes) was 2.21, substantially smaller than that of the passerines considered
426 here. The relative difference in relative leg morphology between the passerines and tinamou could be

427 one of the determining factors resulting in the variability in take-off mechanics between the clades of
428 birds.

429 The kinematics used to drive the take-off simulation were informed by previously obtained XROMM
430 data of the zebra finch take-off leaps [1]. In this study, the use of the tantalum bead markers, detailed
431 bone surface geometry from high resolution µCT, and anatomical-functional relationships [31, 54]
432 were all used to increase repeatability in tracking 3D skeletal kinematics and reduce the influence of
433 the user during scientific rotoscoping [42]. Across the two kinematics trials, the difference between
434 the originally published orientation angles of the femur, tibiotarsus and tarsometatarsus was smallest
435 about FE and ABAD axes of the bones, with mean differences ranging from 0.6±0.5° to 3.3±2.7°. The
436 degree of freedom most difficult to determine during scientific rotoscoping was IER due to the
437 cylindrical shape of the long bones. Predictably, the largest difference was observed when comparing
438 the bone IER orientations, with mean differences in IER orientations across the three long bones
439 ranging from 7.3±4.8° to 11.5±6.3°. Differences in bone locations between the two methods were
440 minimal, mean differences across all three long bones ranged between 185 – 333 microns.

441 Due to the limited number of specimens in which sufficient bones had had a minimum of three
442 tantalum markers attached, only two sets of kinematics trials were used in this study. However, by
443 pairing each set of kinematic trials with nine sets of kinetics trials, we maximised the variability in take-
444 off conditions studied here. Future studies, using XROMM to capture detailed kinematics of passerines
445 should ensure that at least one of the long bones includes at least 3 markers to reduce the reliance on
446 the user during scientific rotoscoping. The simulations here included IER motion of the knee and ankle
447 joints, however the active muscle actuation of these degrees of freedom was not considered in line
448 with previous studies and under the assumption that typically small moments are balanced by passive
449 structures such as ligaments [37, 55]. Previous studies reported the take-off velocity of the zebra finch
450 to be around 1.7m/s [2, 6] which is faster than the take-off velocity, measured here from the XROMM
451 data which ranged between 1.08-1.39 m/s. Previously published studies measuring the kinematics of

452 animal subjects using implanted markers have reported the markers causing a limp [14]. The
453 comparatively slower take-off velocities reported here could thus be attributed to a response to the
454 implantation of the tantalum bead markers on the hindlimb bones. However, varying levels of
455 motivation between experimental conditions may also explain the observed difference and the similar
456 protocols using tantalum bead markers have been used to study a range of motor behaviours in birds
457 [46, 56, 57]. This study did not include the mechanics of phalanges in the analysis, as the take-off
458 trajectories of the hindlimb are defined primarily by the motion at the more proximal hindlimb joints
459 where also more substantial joint moments are generated. Future studies which may consider hind
460 limb mechanics during landing, when the detailed mechanics of foot are likely to play a more
461 important role, should aim to capture the detailed kinematics of the phalanges.

462 This study considered the maximal moment generating capacity of the muscles, taking into account
463 the muscle maximum isometric force and instantaneous moment arm throughout the take-off leap
464 and contrasted these to the external moments applied to the joints of the hind limb. In this way
465 general patterns of mechanical requirement and hindlimb muscles capability to meet the
466 requirements of a take-off leap were analysed. Although the sensitivity of muscle moment generating
467 capacity with respect to uncertainty in the definition of muscle geometry was not directly investigated
468 in this study, a thorough sensitivity analysis was performed for pelvic muscles in the magpie hindlimb
469 model that was the basis for the current study [10], which, given the similarity in overall hindlimb
470 design and specific hindlimb bone morphology, can reasonably be expected to remains valid for the
471 musculature of the zebra finch model here. Though the determination of the detailed muscle
472 activation patterns to balance the external moments was not within the scope of the current study,
473 further analyses of the biomechanical model (such as static optimisation [15, 32, 37]) would help to
474 further elucidate the detailed activation patterns of individual muscles as well as providing estimates
475 for the likely bon-on-one joint contact forces being transferred at le large joints of the avian hind limb
476 during a take-off leap.

477 This study is the first to establish the biomechanical requirements of the hindlimb of a flying bird as it
478 takes to the air. We present biomechanical conditions that hindlimbs of passerines, a clade of birds
479 that include over half of all avian species, experience during take-off. The zebra finch take-off leap is
480 primarily hip and ankle driven, which is in direct contrast to ostrich running mechanics which indicates
481 avian running is a primarily knee driven activity. The ability of the zebra finch muscles to produce over
482 double the mechanical requirements at the ankle and knee axes and about 20% more than the
483 requirements about the hip FE axis along with the suspected use of biarticular muscles and passive
484 structures is consistent with the hypothesis that the take-off leap as reported here is an optimized
485 way for the zebra finch to take to the air. Striking similarities in ground reaction forces and relative leg
486 morphology of multiple passerines suggest that the take-off behaviour described here could be shared
487 across all passerines, despite differences in mass by two orders of magnitude.

488 **Acknowledgements**

489 We would like to acknowledge the skill, hard work, and patience of the bird handlers Lloyd and Rose
490 Buck who helped with the collection of the ground reaction force data of the crow and raven. This
491 work was supported by the Natural Environmental Research Council [grant number NE/L002531/1]
492 and grants from the UMR 7179, l Action Transversale du Muséum National d Histoire Naturelle formes
493 possibles, formes réalisées and from Ecole Doctorale Frontières du Vivant and Bettencourt-Schueller
494 Foundation fellowships as well as the National Science Foundation [grant nos IOS-0923606 and IOS-
495 0919799]. Travels were paid by the UMR 7179.

496

Tables

Table 1 Musculotendon units included in the musculoskeletal model of the zebra finch, grouped by which joints they cross; H, K and A denote the hip, knee and ankle joints, respectively. Muscles which are categorised under two joints are biarticular. Maximum isometric force was calculated by scaling the maximum isometric force of the corresponding muscles of the magpie by mass [10].

Abbreviation	Muscle name	Joints	Maximum isometric force [N]
MCFC	*M. caudofemoralis pars caudalis*	H	0.154
MFCLA	*M. flexor cruris lateralis pars accessoria*	H	0.250
MISF1	*M. ischiofemoralis 1*	H	0.259
MISF2	*M. ischiofemoralis 2*	H	0.259
MISF3	*M. ischiofemoralis 3*	H	0.259
MITC1	*M. iliotrochantericus caudalis 1*	H	0.396
MITC2	*M. iliotrochantericus caudalis 2*	H	0.396
MITC3	*M. iliotrochantericus caudalis 2*	H	0.396
MITCR	*M. iliotrochantericus cranialis*	H	0.003
MITM	*M. iliotrochantericus medius*	H	0.057
MOL	*M. obturatorius lateralis*	H	0.112
MOM	*M. obturatorius medialis*	H	0.431
MPIFL	*M. puboischiofemoralis pars lateralis*	H	0.388
MPIFM	*M. puboischiofemoralis pars medialis*	H	0.448
MFCLP	*M. flexor cruris lateralis pars pelvica*	H, K	0.346
MFCM	*M. flexor cruris medialis*	H, K	0.238
MIC	*M. iliotibialis cranialis*	H, K	0.218
MIF	*M. iliofibularis*	H, K	0.458
MILcaudal1	*M. iliotibialis lateralis caudalis 1*	H, K	0.254
MILcaudal2	*M. iliotibialis lateralis caudalis 2*	H, K	0.254
MILcaudal3	*M. iliotibialis lateralis caudalis 3*	H, K	0.254
MILcranial1	*M. iliotibialis lateralis cranialis 1*	H, K	0.036
MILcranial2	*M. iliotibialis lateralis cranialis 2*	H, K	0.036
MILcranial3	*M. iliotibialis lateralis cranialis 3*	H, K	0.036
MFTI	*M. femorotibialis intermedius*	K	0.614
MFTL	*M. musculus femorotibialis lateralis*	K	0.013
MFTM	*M. femorotibialis medialis*	K	0.490
MFHL	*M. flexor hallucis longus*	K, A	0.843
MFPD2	*M. flexor perforates digiti 2*	K, A	0.357
MFPD3	*M. flexor perforates digiti 3*	K, A	0.362
MFPD4	*M. flexor perforates digiti 4*	K, A	0.483
MFPPD2	*M. flexor perforans et perforates digiti 2*	K, A	0.236

MGI	*M. gastrocnemius pars intermedia*	K, A	0.621
MGL	*M. gastroc-nemius pars lateralis*	K, A	1.824
MTCF	*M. tibialis cranialis caput femorale*	K, A	0.385
MEDL	*M. extensor digitorum longus*	A	0.031
MFB	*M. fibularis brevis*	A	0.366
MFDL	*M. flexor digitorum longus*	A	1.003
MFL	*M. fibularis longus*	A	0.861
MFPPD3	*M. flexor perforans et perforates digiti 3*	A	0.894
MGM	*M. gastrocnemius pars medialis*	A	1.153
MP	*M. plantaris*	A	0.079
MTCT	*M. tibialis cranialis caput tibiale*	A	0.516

502

503 Table 2. Key morphometric parameters of zebra finch (Taeniopygia guttata), starling (Sturnis
504 vulgaris), crow (Corvus corone), and raven (Corvus corax).

species	mass [g]	femur length (L_{fem}) [cm]	tibiotarsus length (L_{tib}) [cm]	tarsometatarsus length (L_{tars}) [cm]	digit III length [cm]	hindlimb length [cm]	hindlimb index ((L_{tars} + L_{tib})/ L_{fem})
zebra finch	15.4	1.40	2.24	1.46	1.10	6.2	2.64
starling [3]	77.3	2.53	4.37	2.82			2.84
crow	440	5.28	8.74	5.77			2.75
raven	1100	6.92	11.42	6.80			2.63

505

506 Table 3 External joint moments and total muscle moment generating capacities of the zebra finch at
507 the instances at which the peak external joint moments occur. To actively power the take-off leap by
508 muscle action, the combined(total) moment generating capacity of all muscles must at least reach if
509 not exceed the level of the external joint moments . Positive moments act in extension, external
510 rotation, and adduction, while negative moments act in flexion, internal rotation, and abduction.

joint DoF	joint moment [BWL] (requirement)	total muscle moment generating capacity [BWL] (capacity to meet requirement)
ankle extension	0.66±0.04	1.18
knee extension	-0.38±0.05	-0.67
hip extension	0.68±0.05	0.81
hip internal rotation	-0.27±0.07	-0.75
hip abduction	-0.20±0.07	-0.12

511

Figure captions

Figure 1 The musculoskeletal model of the left zebra finch hindlimb included 43 musculotendon units. A) Muscles that either cross the hip or knee joint and biarticular muscles crossing both hip and knee joints are shown in a caudo-lateral view. B) Anterior and C) posterior view of muscles crossing the ankle joint and biarticular muscles crossing both knee and ankle joints. For an explanation of the abbreviations of the muscles used here, please refer to Table 1.

Figure 2 Schematic demonstrating the process of morphing the musculature from the magpie to the zebra finch hindlimb. To allow for a better visual comparison of the bones which differ by almost a factor of two in size, the bone surfaces depicted here are isotopically scaled by the reciprocal of the square root of their respective surface area. **A** Establishing an elastic mapping by comparing magpie and zebra finch bone surfaces. Here, magpie bones were first registered to the corresponding zebra finch bone using non-rigid iterative closest point (ICP) registration [39]. Following non-rigid registration, the rigid transformation and isotropic scaling parameters were recovered using Ordinary Procrustes Analysis (OPA) computed between the vertices of the original magpie bone surface and the vertices of the magpie bone surface that was elastically registered to the respective zebra finch bone. This step was encoded in a 4x4 homogeneous transformation matrix. The remaining difference between the positions of the OPA mapped vertices and their elastically registered counterparts was captured in a dense deformation field. **B** Application of the elastic mapping to muscle attachment and via point data. The homogeneous transformation matrix and the dense deformation field were then applied to all attachment and via points of the magpie muscles associated to the respective bone surface, resulting in an elastic registration of these structures to the zebra finch model.

Figure 3 Force and moment diagram for the zebra finch hindlimb, including the pelvis, femur, tibiotarsus and tarsometatarsus in a lateral view. The musculoskeletal model described the hip, knee and ankle as three, two and two degree of freedom joints respectively. The straight black arrow on the perch represents the ground reaction force acting through the centre of the perch. Curved arrows reflect external moments acting at the joints and are colour coded such that the orange arrows identify the moment about the joint's flexion/extension axes, blue arrows identify moments about a joints' internal/external rotation axis, and green arrow identifies the moments about the joints' ab/adduction axis. At the hip, the ground reaction forces consistently result in flexion, abduction and an internal rotation moments throughout the leap cycles. At the knee and ankle joints, the ground reaction forces result in extension, and flexion moments, respectively.

Figure 4 Lateral view of right zebra finch hindlimb throughout the normalised take-off leap cycle. The duration of the take-off jump duration ranged from 62 to 67 ms while all of the ankle, knee, and hip joint undergo substantial extension.

Figure 5 External joint moments at the hip, knee and ankle together with the total moment generating capacity of the muscles, plotted over normalised leap cycle time. Solid lines depict the mean external joint moments (requirements), bands depict ±2.5 standard deviations, while dashed lines depict the total moment generating capacity of the muscles (capacity). Colours are used to differentiate the axis around which the moments act, with orange representing flexion/extension, green ab/adduction, and blue internal/external rotation. Positive moments represent (internal/external) moments that act to extend, adduct, and internally rotate, respectively.

References

[1] Provini, P. & Abourachid, A. 2018 Whole-body 3D kinematics of bird take-off: key role of the legs to propel the trunk. *The Science of Nature* **105**, 12. (doi:10.1007/s00114-017-1535-8).

[2] Provini, P., Tobalske, B.W., Crandell, K.E. & Abourachid, A. 2012 Transition from leg to wing forces during take-off in birds. *J Exp Biol* **215**, 4115-4124. (doi:10.1242/jeb.074484).

[3] Earls, K.D. 2000 Kinematics and mechanics of ground take-off in the starling Sturnis vulgaris and the quail Coturnix coturnix. *Journal of Experimental Biology* **203**, 725-739.

[4] Bonser, R. & Rayner, J. 1996 Measuring leg thrust forces in the common starling. *The Journal of Experimental Biology* **199**, 435-439.

[5] Heppner, F.H. & Anderson, J.G.T. 1985 Leg Thrust Important in Flight Take-Off in the Pigeon. *Journal of Experimental Biology* **114**, 285-288.

[6] Tobalske, B.W. 2004 Take-off mechanics in hummingbirds (Trochilidae). *Journal of Experimental Biology* **207**, 1345-1352. (doi:10.1242/jeb.00889).

[7] Selvatti, A.P., Gonzaga, L.P. & Russo, C.A.d.M. 2015 A Paleogene origin for crown passerines and the diversification of the Oscines in the New World. *Molecular Phylogenetics and Evolution* **88**, 1-15. (doi:https://doi.org/10.1016/j.ympev.2015.03.018).

[8] Ricklefs, R.E. 2012 Species richness and morphological diversity of passerine birds. *Proceedings of the National Academy of Sciences* **109**, 14482. (doi:10.1073/pnas.1212079109).

[9] Raikow, R.J. 1987 Hindlimb Myology and Evolution of the Old World Suboscine Passerine Birds (Acanthisittidae, Pittidae, Philepittidae, Eurylaimidae). *Ornithological Monographs*, iii-81. (doi:10.2307/40166726).

[10] Meilak, E.A., Gostling, N.J., Palmer, C. & Heller, M.O. 2021 On the 3D Nature of the Magpie (Aves: Pica pica) Functional Hindlimb Anatomy During the Take-Off Jump. *Frontiers in Bioengineering and Biotechnology* **9**. (doi:10.3389/fbioe.2021.676894).

[11] Bergmann, G., Deuretzbacher, G., Heller, M., Graichen, F., Rohlmann, A., Strauss, J. & Duda, G.N. 2001 Hip contact forces and gait patterns from routine activities. *Journal of Biomechanics* **34**, 859-871. (doi:http://dx.doi.org/10.1016/S0021-9290(01)00040-9).

[12] Heller, M.O., Bergmann, G., Deuretzbacher, G., Dürselen, L., Pohl, M., Claes, L., Haas, N.P. & Duda, G.N. 2001 Musculo-skeletal loading conditions at the hip during walking and stair climbing. *Journal of Biomechanics* **34**, 883-893. (doi:10.1016/S0021-9290(01)00039-2).

[13] Heller, M.O., Taylor, W.R., Perka, C. & Duda, G.N. 2003 The influence of alignment on the musculo-skeletal loading conditions at the knee. *Langenbeck's Archives of Surgery* **388**, 291-297. (doi:10.1007/s00423-003-0406-2).

[14] Taylor, W.R., Ehrig, R.M., Heller, M.O., Schell, H., Seebeck, P. & Duda, G.N. 2006 Tibio-femoral joint contact forces in sheep. *Journal of Biomechanics* **39**, 791-798. (doi:10.1016/j.jbiomech.2005.02.006).

[15] Delp, S.L., Anderson, F.C., Arnold, A.S., Loan, P., Habib, A., John, C.T., Guendelman, E. & Thelen, D.G. 2007 OpenSim: open-source software to create and analyze dynamic simulations of movement. *IEEE transactions on bio-medical engineering* **54**, 1940-1950. (doi:10.1109/tbme.2007.901024).

[16] Allen, V.R., Kilbourne, B.M. & Hutchinson, J.R. 2021 The evolution of pelvic limb muscle moment arms in bird-line archosaurs. *Science Advances* **7**, eabe2778. (doi:10.1126/sciadv.abe2778).

[17] Hutchinson, J.R., Anderson, F.C., Blemker, S.S. & Delp, S.L. 2005 Analysis of hindlimb muscle moment arms in Tyrannosaurus rex using a three-dimensional musculoskeletal computer model: implications for stance, gait, and speed. *Paleobiology* **31**, 676-701.

[18] Bishop, P.J., Hocknull, S.A., Clemente, C.J., Hutchinson, J.R., Farke, A.A., Barrett, R.S. & Lloyd, D.G. 2018 Cancellous bone and theropod dinosaur locomotion. Part III—Inferring posture and locomotor biomechanics in extinct theropods, and its evolution on the line to birds. *PeerJ* **6**, e5777. (doi:10.7717/peerj.5777).

602 [19] Duda, G.N., Eckert-Hübner, K., Sokiranski, R., Kreutner, A., Miller, R. & Claes, L. 1997 Analysis of
603 inter-fragmentary movement as a function of musculoskeletal loading conditions in sheep. *Journal of*
604 *Biomechanics* **31**, 201-210. (doi:https://doi.org/10.1016/S0021-9290(97)00127-9).
605 [20] Goetz, J.E., Derrick, T.R., Pedersen, D.R., Robinson, D.A., Conzemius, M.G., Baer, T.E. & Brown,
606 T.D. 2008 Hip joint contact force in the emu (Dromaius novaehollandiae) during normal level
607 walking. *J Biomech* **41**, 770-778. (doi:10.1016/j.jbiomech.2007.11.022).
608 [21] Lund, K. & Hicks, J. 2012 Getting Started with Inverse Dynamics. In *OpenSim Documentation* (
609 [22] Pizzolato, C., Reggiani, M., Modenese, L. & Lloyd, D.G. 2017 Real-time inverse kinematics and
610 inverse dynamics for lower limb applications using OpenSim. *Computer methods in biomechanics*
611 *and biomedical engineering* **20**, 436-445. (doi:10.1080/10255842.2016.1240789).
612 [23] Bishop, P.J., Falisse, A., De Groote, F. & Hutchinson, J.R. 2021 Predictive simulations of
613 musculoskeletal function and jumping performance in a generalized bird. *Integrative Organismal*
614 *Biology*. (doi:10.1093/iob/obab006).
615 [24] Rankin, J.W., Rubenson, J. & Hutchinson, J.R. 2016 Inferring muscle functional roles of the
616 ostrich pelvic limb during walking and running using computer optimization. *Journal of The Royal*
617 *Society Interface* **13**. (doi:10.1098/rsif.2016.0035).
618 [25] Rubenson, J., Lloyd, D.G., Besier, T.F., Heliams, D.B. & Fournier, P.A. 2007 Running in ostriches
619 (Struthio camelus): three-dimensional joint axes alignment and joint kinematics. *Journal of*
620 *Experimental Biology* **210**, 2548-2562. (doi:10.1242/jeb.02792).
621 [26] Rubenson, J., Lloyd, D.G., Heliams, D.B., Besier, T.F. & Fournier, P.A. 2010 Adaptations for
622 economical bipedal running: the effect of limb structure on three-dimensional joint mechanics.
623 *Journal of The Royal Society Interface*. (doi:10.1098/rsif.2010.0466).
624 [27] Kambic, R.E., Roberts, T.J. & Gatesy, S.M. 2014 Long-axis rotation: a missing degree of freedom
625 in avian bipedal locomotion. *J Exp Biol* **217**, 2770-2782. (doi:10.1242/jeb.101428).
626 [28] Kambic, R.E., Roberts, T.J. & Gatesy, S.M. 2017 3-D range of motion envelopes reveal interacting
627 degrees of freedom in avian hind limb joints. *Journal of Anatomy* **231**, 906-920.
628 (doi:doi:10.1111/joa.12680).
629 [29] Verstappen, M., Aerts, P. & De Vree, F. 1998 Functional morphology of the hindlimb
630 musculature of the black-billed magpie, Pica pica (Aves, Corvidae). *Zoomorphology* **118**, 207-223.
631 (doi:10.1007/s004350050070).
632 [30] Hudson, G.E. 1937 Studies on the Muscles of the Pelvic Appendage in Birds. *The American*
633 *Midland Naturalist* **18**, 1-108. (doi:10.2307/2420619).
634 [31] Ehrig, R.M. & Heller, M.O. 2019 On intrinsic equivalences of the finite helical axis, the
635 instantaneous helical axis, and the SARA approach. A mathematical perspective. *Journal of*
636 *Biomechanics* **84**, 4-10. (doi:https://doi.org/10.1016/j.jbiomech.2018.12.034).
637 [32] Seth, A., Sherman, M., Reinbolt, J.A. & Delp, S.L. 2011 OpenSim: a musculoskeletal modeling and
638 simulation framework for in silico investigations and exchange. *Procedia IUTAM* **2**, 212-232.
639 (doi:https://doi.org/10.1016/j.piutam.2011.04.021).
640 [33] Trepczynski, A., Kutzner, I., Kornaropoulos, E., Taylor, W.R., Duda, G.N., Bergmann, G. & Heller,
641 M.O. 2012 Patellofemoral joint contact forces during activities with high knee flexion. *Journal of*
642 *Orthopaedic Research* **30**, 408-415. (doi:10.1002/jor.21540).
643 [34] Schlager, S. 2015 *mesheR: Meshing operations on triangular meshes*.
644 [35] Yushkevich, P.A., Piven, J., Hazlett, H.C., Smith, R.G., Ho, S., Gee, J.C. & Gerig, G. 2006 User-
645 guided 3D active contour segmentation of anatomical structures: Significantly improved efficiency
646 and reliability. *NeuroImage* **31**, 1116-1128. (doi:https://doi.org/10.1016/j.neuroimage.2006.01.015).
647 [36] McNeel, R. 2020 Rhinoceros 3D, Version 4.0. *Robert McNeel & Associates, Seattle, WA*.
648 [37] Seth, A., Hicks, J.L., Uchida, T.K., Habib, A., Dembia, C.L., Dunne, J.J., Ong, C.F., DeMers, M.S.,
649 Rajagopal, A., Millard, M., et al. 2018 OpenSim: Simulating musculoskeletal dynamics and
650 neuromuscular control to study human and animal movement. *PLOS Computational Biology* **14**,
651 e1006223. (doi:10.1371/journal.pcbi.1006223).

[38] Cox, S.M., Easton, K.L., Lear, M.C., Marsh, R.L., Delp, S.L. & Rubenson, J. 2019 The Interaction of Compliance and Activation on the Force-Length Operating Range and Force Generating Capacity of Skeletal Muscle: A Computational Study using a Guinea Fowl Musculoskeletal Model. *Integrative Organismal Biology* **1**. (doi:10.1093/iob/obz022).
[39] Manu. 2021 nonrigidICP. *MATLAB Central File Exchange*.
[40] Fedorov, A., Beichel, R., Kalpathy-Cramer, J., Finet, J., Fillion-Robin, J.-C., Pujol, S., Bauer, C., Jennings, D., Fennessy, F., Sonka, M., et al. 2012 3D Slicer as an image computing platform for the Quantitative Imaging Network. *Magn Reson Imaging* **30**, 1323-1341. (doi:10.1016/j.mri.2012.05.001).
[41] Veldpaus, F.E., Woltring, H.J. & Dortmans, L.J.M.G. 1988 A least-squares algorithm for the equiform transformation from spatial marker co-ordinates. *Journal of Biomechanics* **21**, 45-54. (doi:https://doi.org/10.1016/0021-9290(88)90190-X).
[42] Brainerd, E.L., Baier, D.B., Gatesy, S.M., Hedrick, T.L., Metzger, K.A., Gilbert, S.L. & Crisco, J.J. 2010 X-ray reconstruction of moving morphology (XROMM): precision, accuracy and applications in comparative biomechanics research. *Journal of Experimental Zoology Part A: Ecological Genetics and Physiology* **313A**, 262-279. (doi:doi:10.1002/jez.589).
[43] Semechko, A. 2021 Rigid body parameters of closed surface meshes.
[44] Parslew, B., Sivalingam, G. & Crowther, W. 2018 A dynamics and stability framework for avian jumping take-off. *Royal Society Open Science* **5**, 181544. (doi:10.1098/rsos.181544).
[45] Daley Monica, A. & Biewener Andrew, A. 2011 Leg muscles that mediate stability: mechanics and control of two distal extensor muscles during obstacle negotiation in the guinea fowl. *Philosophical Transactions of the Royal Society B: Biological Sciences* **366**, 1580-1591. (doi:10.1098/rstb.2010.0338).
[46] Allen, V.R., Kambic, R.E., Gatesy, S.M. & Hutchinson, J.R. 2017 Gearing effects of the patella (knee extensor muscle sesamoid) of the helmeted guineafowl during terrestrial locomotion. *Journal of Zoology* **303**, 178-187. (doi:doi:10.1111/jzo.12485).
[47] Carr, J.A., Ellerby, D.J. & Marsh, R.L. 2011 Function of a large biarticular hip and knee extensor during walking and running in guinea fowl (Numida meleagris). *The Journal of Experimental Biology* **214**, 3405. (doi:10.1242/jeb.060335).
[48] Trepczynski, A., Kutzner, I., Schwachmeyer, V., Heller, M.O., Pfitzner, T. & Duda, G.N. 2018 Impact of antagonistic muscle co-contraction on in vivo knee contact forces. *Journal of NeuroEngineering and Rehabilitation* **15**, 101. (doi:10.1186/s12984-018-0434-3).
[49] Hutchinson, J.R., Rankin, J., Rubenson, J., Rosenbluth, K.H., Siston, R.A. & Delp, S.L. 2015 Musculoskeletal modelling of an ostrich (Struthio camelus) pelvic limb: influence of limb orientation on muscular capacity during locomotion. *Peerj* **3**, 52. (doi:10.7717/peerj.1001).
[50] Hutchinson, J.R., Ng-Thow-Hing, V. & Anderson, F.C. 2007 A 3D interactive method for estimating body segmental parameters in animals: Application to the turning and running performance of Tyrannosaurus rex. *Journal of Theoretical Biology* **246**, 660-680. (doi:10.1016/j.jtbi.2007.01.023).
[51] Mayr, G. 2016 Variations in the hypotarsus morphology of birds and their evolutionary significance. *Acta Zoologica* **97**, 196-210. (doi:https://doi.org/10.1111/azo.12117).
[52] Field, D.J., Bercovici, A., Berv, J.S., Dunn, R., Fastovsky, D.E., Lyson, T.R., Vajda, V. & Gauthier, J.A. 2018 Early Evolution of Modern Birds Structured by Global Forest Collapse at the End-Cretaceous Mass Extinction. *Current Biology*. (doi:https://doi.org/10.1016/j.cub.2018.04.062).
[53] !!! INVALID CITATION !!! [3, 49].
[54] Ehrig, R.M., Taylor, W.R., Duda, G.N. & Heller, M.O. 2007 A survey of formal methods for determining functional joint axes. *Journal of Biomechanics* **40**, 2150-2157. (doi:https://doi.org/10.1016/j.jbiomech.2006.10.026).
[55] Marieswaran, M., Sikidar, A., Goel, A., Joshi, D. & Kalyanasundaram, D. 2018 An extended OpenSim knee model for analysis of strains of connective tissues. *BioMedical Engineering OnLine* **17**, 42. (doi:10.1186/s12938-018-0474-8).

703 [56] Brown, N.P., Bertocci, G.E., Cheffer, K.A. & Howland, D.R. 2018 A three dimensional multiplane
704 kinematic model for bilateral hind limb gait analysis in cats. *PLOS ONE* **13**, e0197837.
705 (doi:10.1371/journal.pone.0197837).
706 [57] Kilbourne, B.M., Andrada, E., Fischer, M.S. & Nyakatura, J.A. 2016 Morphology and motion:
707 hindlimb proportions and swing phase kinematics in terrestrially locomoting charadriiform birds. *J*
708 *Exp Biol* **219**, 1405-1416. (doi:10.1242/jeb.124081).

709

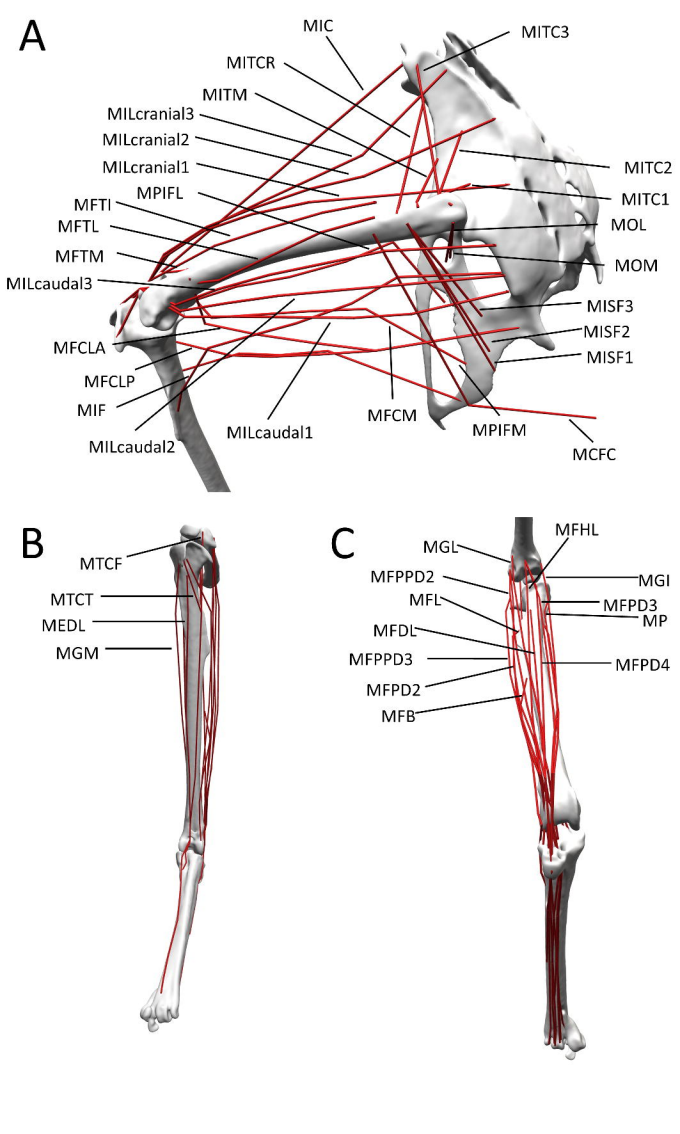
A
MIC
MITC3
MITCR
MITM
MILcranial3
MILcranial2
MILcranial1
MPIFL
MFTI
MFTL
MFTM
MILcaudal3
MFCLA
MFCLP
MIF
MILcaudal2
MILcaudal1
MFCM
MPIFM
MCFC
MITC2
MITC1
MOL
MOM
MISF3
MISF2
MISF1
B
MTCF
MTCT
MEDL
MGM
C
MFHL
MGL
MFPPD2
MFL
MFDL
MFPPD3
MFPD2
MFB
MGI
MFPD3
MP
MFPD4

A establish elastic mapping by comparing magpie and zebra finch bone surfaces

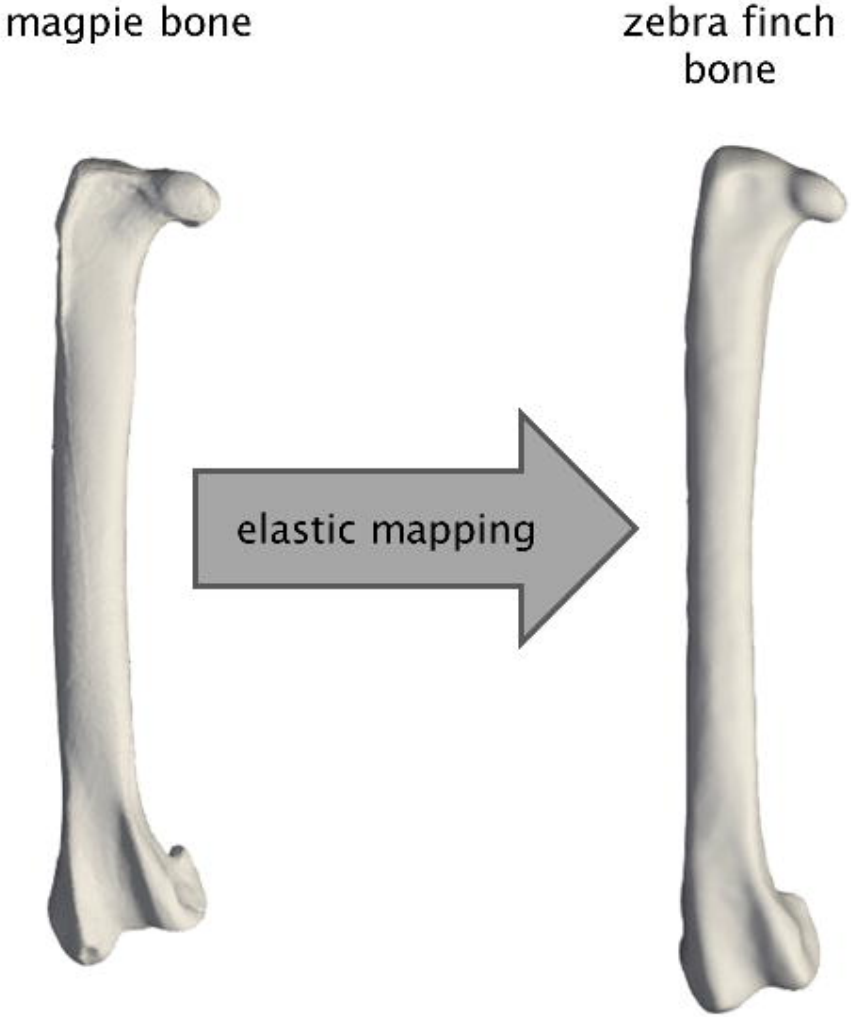

B apply elastic mapping to muscle attachment and via point data

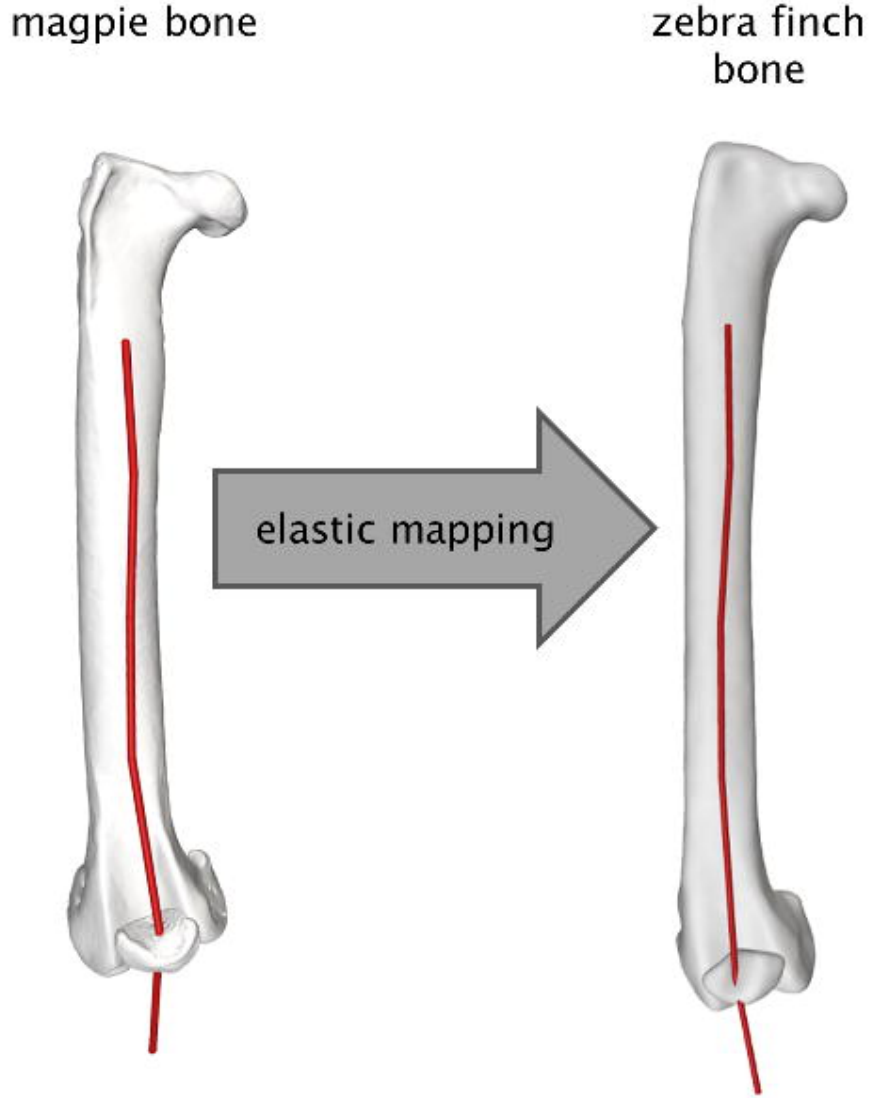

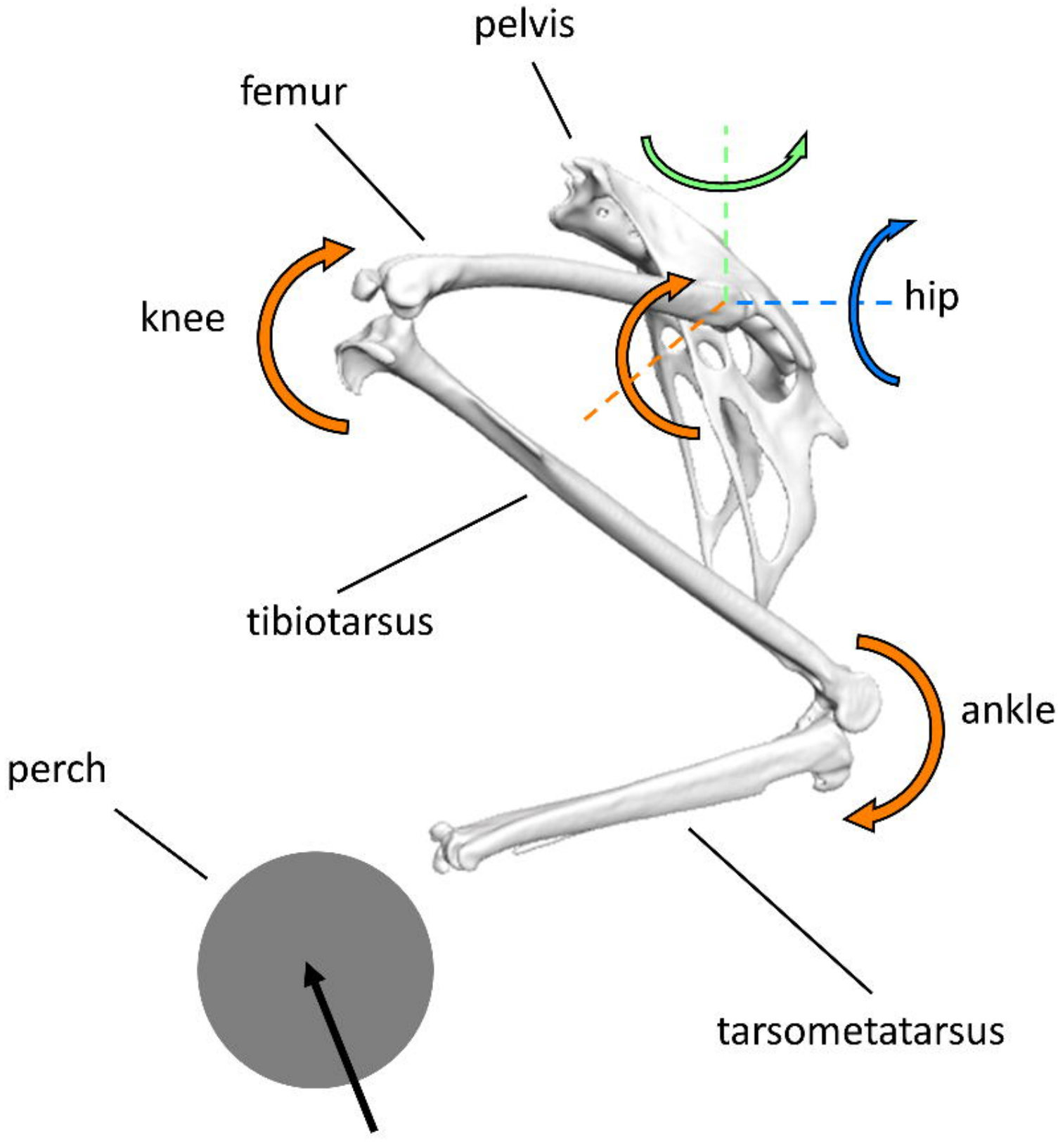
pelvis
femur
knee
hip
tibiotarsus
ankle
perch
tarsometatarsus

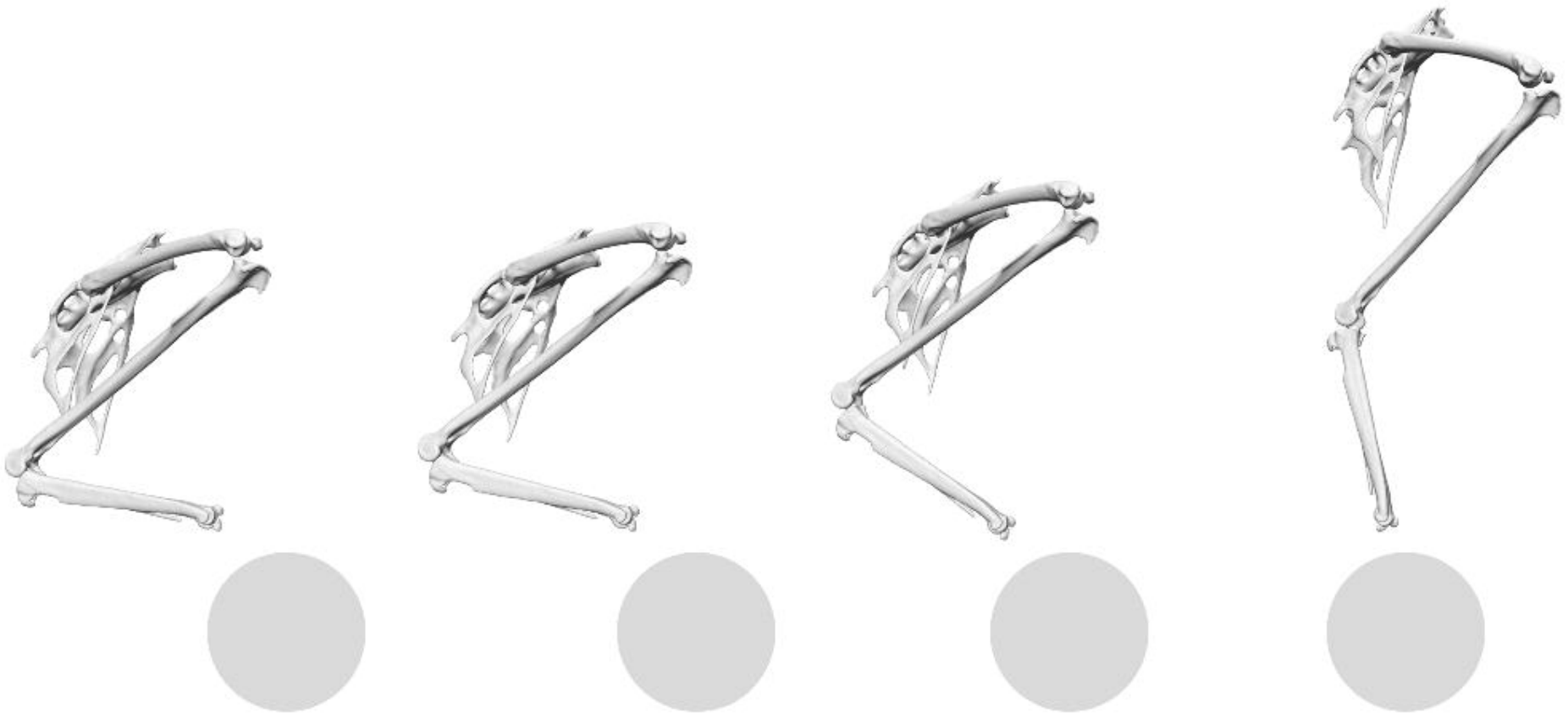
T [%]
0%
33%
66%
100%

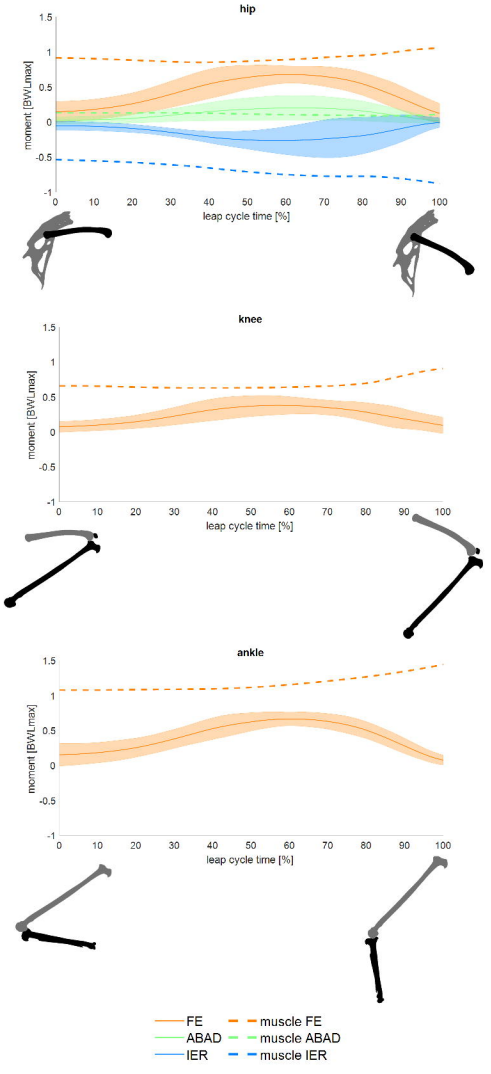
hip
moment [BW*Lmax]
leap cycle time [%]
knee
moment [BW*Lmax]
leap cycle time [%]
ankle
moment [BW*Lmax]
leap cycle time [%]
FE
ABAD
IER
muscle FE
muscle ABAD
muscle IER